On Bubbles Rising Through Suspensions of Solid Particles

Lisa A. Mondy, Charles Retallack, Kyle Thompson, Jeremy Barney, and Anne Grillet
Sandia National Laboratories, Albuquerque, NM 87185

Alan L. Graham
Los Alamos National Laboratory, Los Alamos, NM 87145

DOI 10.1002/aic.11440
Published online February 21, 2008 in Wiley InterScience (www.interscience.wiley.com).

Individual bubbles rising through suspensions of spherical particles neutrally buoyant in viscous Newtonian liquids are tracked with real time radiography. The effects of the containing cylinder, suspended particle, and bubble sizes are reported for particle volume fractions ranging from 0.20 to 0.50. In the most concentrated suspensions, the effect of the bottom surface is felt by the bubble much farther into the suspension than would be true for a single-phase Newtonian liquid. Corrected for wall effects, the apparent viscosity felt by the bubbles is independent of the relative size of the bubble to the particle over a wide range of parameters, and is approximately linear with the suspended particle volume fraction, in contrast to the exponential dependence derived in conventional rheometry. Finally, in the most concentrated suspensions, the bubble deforms to a prolate spheroidal shape despite the lack of significant inertial effects or a viscoelastic suspending liquid. © 2008 American Institute of Chemical Engineers* *AIChE J,* 54: 862–871, 2008

Keywords: bubble phenomena, settling/sedimentation, suspensions

Introduction

The characterization of the behavior of single bubbles rising in suspensions of solid particles is important to applications ranging from design of slurry bubble column reactors to flotation separation in minerals processing to degassing of filled polymers or ceramic precursors. Also because of the increasing interest in multiphase materials in micro fluidics applications, there is a need to understand the behavior of bubbles and suspended particles interacting with each other and walls when the distance between walls is only a few times larger than the characteristic dimension of the bubbles or particles. Bubble rise behavior has been extensively studied in Newtonian fluids[1,2] and in non-Newtonian fluids.[3] Sokolichin et al. have reviewed more recently drag correlations for air bubbles rising in water.[4] The drag on a bubble rising through a suspension of solid particles has been reported less often. Bubble–particle interactions, where the bubble is much larger than the solid particles, have been studied for the mining industry, with focus on the capturing of these particles by the bubble through collision and adhesion.[5–7] The rise of bubbles through suspended particles has also been studied for applications in gas-liquid-solid fluidization systems.[2,8] Darton and Harrison collected the rise velocities of spherical cap bubbles (5–25 mm in diameter) in fluidized beds of either 500-μm or 1-mm diameter sand particles.[9] They determined an effective bed viscosity that varied with particle size and bed expansion. Tsuchiya et al. pointed out problems in the concept of a small bubble experiencing a single effective viscosity of an assumed homogeneous bed, but showed that this concept of a Newtonian analogy could apply for larger 12- to 17-mm diameter bubbles in a bed of 0.55-mm diameter particles.[10,11] This effective media analogy has been used by many in modeling gas-liquid-solid flu-

Correspondence concerning this article should be addressed to L. A. Mondy at lamondy@sandia.gov.

idization systems (e.g., Li and Prakash,[12] Zhang et al.,[13] Buwa and Ranade[14]). Kenny and McLaughlin looked at the rise velocity of smaller bubbles (0.6–9 mm in diameter) in a fluidized bed of particles of a similar size (0.8 mm in diameter) over a wide range of solid volume fractions (0.15–0.52).[15] They determined that a semiempirical correlation treating the fluidized bed as an effective Newtonian media was an accurate representation for solid volume fractions up to 0.45.

The notion that a particle might experience a suspension of similarly sized particles as an effective Newtonian continum was also explored earlier using a single falling sphere, rather than a rising bubble. Mondy et al. showed that neutrally buoyant suspensions subjected to falling ball viscometry yielded an effective Newtonian viscosity, with concomitant wall effects, if the falling ball was at least as large as the suspended particles and the volume fraction of solids was under 0.30.[16] At larger volume fractions, wall effects were seen to be larger than expected for a Newtonian single phase fluid. Poletto and Joseph determined an effective drag law for a test sphere in a fluidized bed using an effective density (the mass average density of the mixture) that was accurate as long as the test sphere was again at least the size of the suspended particles.[17]

The effects of container walls and bottom on the fall of solid spheres through single-phase liquids have been examined extensively,[18–22] as have the effects of walls on the rise of bubbles.[23,24] Clift et al.[1] and Chhabra[3] gave excellent overviews of such work. More recently, the effects of the container walls and ends on the velocity of a single sphere falling in a suspension of similarly sized, neutrally buoyant spheres, has also been examined. Kaiser et al. found that wall effects, experienced by the falling ball in a cylinder containing a suspension, begin to deviate from Newtonian behavior both when the suspension becomes highly concentrated and when the falling ball has an eccentric path of descent within the test column.[25] The end effects experienced by falling balls in suspensions have been studied by Reardon et al.[26,27] For a Newtonian liquid in a cylindrical column, end effects generally exist only within one cylinder diameter of the top and bottom of the column. However, falling balls in highly concentrated suspensions experience end effects as many as 13 cylinder diameters from the bottom of a cylindrical column.

Less is known about how a bubble interacts with the ends of the column as it rises through a stationary suspension. The goal here is to address Newtonian and non-Newtonian behavior previously observed in falling ball experiments in suspensions as they apply to similar experiments using rising bubbles as test spheres. We also expand on the experiments of Kenny and McLaughlin[15] to examine the effects of the suspended particle size to rising bubble size ratio d_s/d_f, the suspended particle size to column diameter ratio d_s/D, and the suspended particle volume fraction ϕ.

As will be described in this article, we see enhanced end effects in concentrated suspensions ($\phi = 0.30$ and 0.50), manifested as an extended length of time for the bubble to accelerate to a steady-state velocity in the suspension as opposed to that in a Newtonian single-phase liquid. The suspensions consist of uniformly sized spherical particles neutrally buoyant in an incompressible, viscous, nonpolar, Newtonian liquid. Bubbles (nominal diameter of 5 mm) are injected along the center line of a cylindrical column and allowed to rise freely through the suspensions. Little, if any effects, of surface-active surfaces are expected in these nonaqueous systems. Parameters that were varied include the suspended particle size (0.5–3.175 mm) and column diameter (12.7–44.2 mm). Suspension concentration was also varied to obtain data for dilute, moderate, and highly concentrated suspensions. Bubble size variation was limited by the bubble injection apparatus, and was thus only varied minimally throughout the experiments.

Our preliminary work was described by Mondy et al.[28] There, we were limited to timing the bubbles' rise through transparent suspensions created by matching the index of refraction of the suspended particles to the suspending liquid. Only suspensions of relatively large particles (with relatively few scattering interfaces) yielded suspensions of sufficient transparency for the experiments to be successful.

In this article, we use real-time radiography and, hence, we are able to track the position of the bubbles and calculate the bubble rise velocity along the length of the test column even when filled with opaque suspensions. We are also better able to examine the shape of the bubble. We find that the bubbles remain spherical in suspensions of low to moderate concentration, but become oblong (stretched in the direction of gravity) in the highly concentrated suspensions. Bubble deformation has been discussed in earlier work in systems with significant inertial or confinement effects or in non-Newtonian fluids.[19,29,30]

In the following section, we describe the experimental materials, technique, and procedure. The method of data analysis is detailed in the third section. The fourth section reports the results. Finally, conclusions are presented.

Materials and Methods

Suspensions

Experiments were carried out by introducing a single bubble into a suspension of neutrally buoyant spheres through the base of the containing cylinder (Figure 1). The bubble was then tracked along the vertical length of the cylinder using real-time radiography. The velocity profile of each bubble was then extracted from the X-ray data set.

Suspensions used in the experiments consisted of a disperse phase of spheres and a continuous phase of a Newtonian liquid. Table 1 lists the type of particles used, their nominal density, and nominal diameter. Polystyrene or polymethyl methacrylate (PMMA) spheres were sieved to obtain a nominal average diameter $d_s = 500$ μm or $d_s = 750$ μm, respectively. Larger, individually ground, spheres were also used. Manufacturers' tolerances for the diameter of the PMMA spheres used in the earlier study by Mondy et al.[28] are 1588 $\pm$ 15 microns, and for even larger polystyrene spheres used here are 3175 $\pm$ 51 microns.

Suspensions with disperse phase volume fractions of $\phi = 0.30$ and 0.50 were made with the polystyrene suspended particles ($d_s = 500$ and 3175 μm) in Ucon 50-HB-5100 lubricant (Union Carbide). The temperature of the experiment was adjusted (to about 37°C) until no flotation or settling was detected over several days. An additional suspension ($\phi = 0.50$) was used, consisting of the PMMA spheres

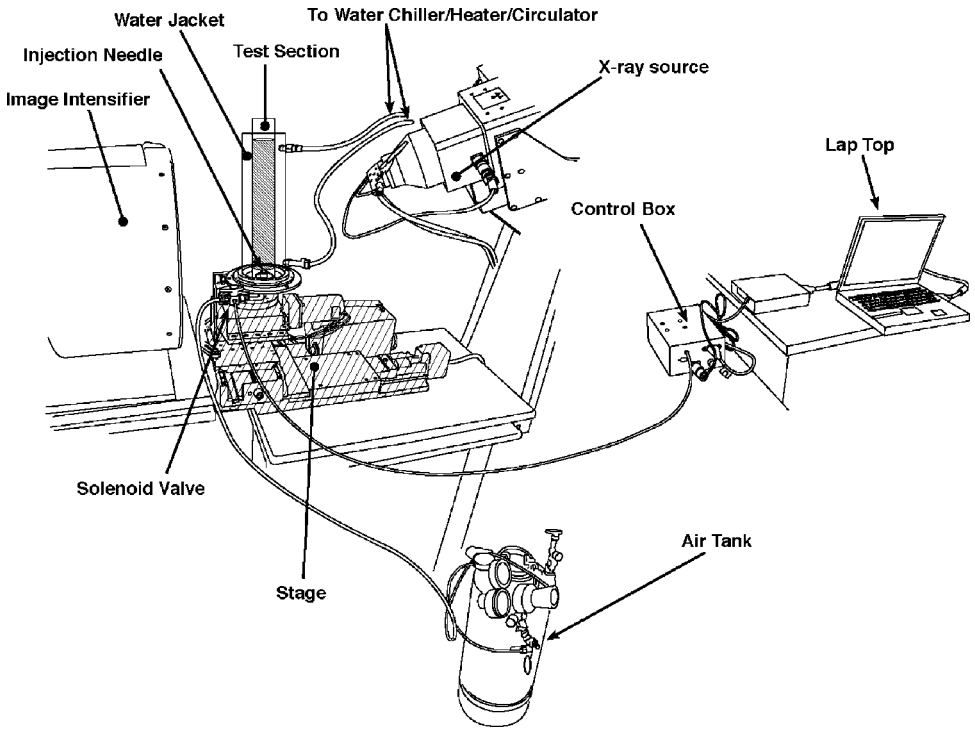

Figure 1. Schematic of experimental apparatus.

(d_s = 750 μm) suspended in a three-component fluid that is density matched to the PMMA at 23°C. This three-component fluid consisted of 15.1% tetrabromoethane (Eastman Kodak), 29.6% Ucon 75-H-90000 (Union Carbide), and 55.3% Triton X-100 (J.T. Baker) by weight.

The suspending liquids have been tested in the past and have shown Newtonian rheology at the low shear rates encountered in these experiments.[31,32] The Ucon 50-HB 5100 has a viscosity of 0.994 Pa s at 37°C. The three-component fluid has a viscosity of 0.827 Pa s at 23°C. Particles were thoroughly mixed into the liquid and allowed to degas at least 24 h prior to experimentation.

Apparatus

Figure 1 is a sketch of the experimental equipment. Four separate test section sizes were used in the experiments. Two test sections had equal diameters of 4.4 cm but varied in height of the material they contained (52.0 and 86.0 cm). The remaining test sections had diameters of 1.3 and 2.2 cm with heights of 25.4 and 48.4 cm, respectively. A computer-activated solenoid valve allowed for a programmable time interval of bubble generation and injection along the axis of the inner cylinder just above the flat bottom surface. Combinations of bubble generation time and air supply pressure were used to control bubble size.

Real-time radiography was used to track bubbles as they traversed the test section. Advantages of this technique include the ability to test opaque suspensions and the elimination of optical distortion that can occur with other imaging techniques. The X-ray source used was an IRT model IXRS160 accompanied by an image intensifier to convert the X-ray projection into an image suitable for optical recording. The X-rays were generated at a nominal power of 80 kV and 1.74 mA for experiments carried out in the 4.4-cm diameter test sections. For both the 2.2- and 1.3-cm diameter columns, the X-ray power generation was modulated to 90 kV and 100 μA.

A computer controlled three-axis stage was used to position the bubble column apparatus relative the X-ray source. The position history of a bubble was recorded using the radiography system along with image capture software. To get adequate spatial resolution to determine the bubble size and shape, only part of the test section was visible at one time when the longer test section was used.

Table 1. Suspended Spheres

		Size Distribution Range, d_s (μm)		
Material	Density (g/cm^3)	Top Sieve	Bottom Sieve	Nominal Diameter Used in Text
Polystyrene	1.05	600	425	500
PMMA	1.18	850	710	750
PMMA (Mondy et al., 2004)	1.17			1588
Polystyrene	1.05			3175

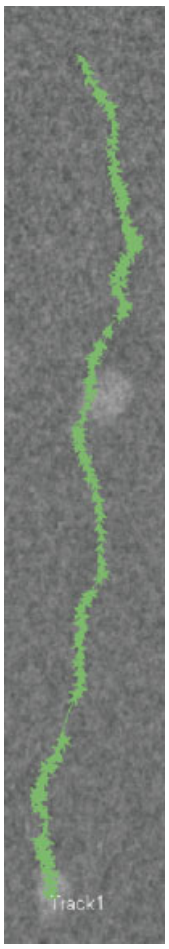

Figure 2. Reconstructed path of the centroid of a bubble traveling through a suspension of 50% of 500 μm diameter particles.

The bubble-like ghost part way up the image is actually an artifact of the background subtraction and not the bubble being tracked. [Color figure can be viewed in the online issue, which is available at www.interscience.wiley.com.]

Procedure

Suspensions were poured into the inner column of the bubble cylinder apparatus and allowed to sit for several hours until the temperature, as measured with a probe, was uniform throughout the inner column to $\pm 0.2^{\circ}$C. Bubbles were then injected into the column on a slow, but continuous, basis and allowed to rise freely through the suspension. The bubbles were generated at sufficiently large time intervals to allow enough distance between bubbles to avoid any bubble to bubble interactions. Image sequences were captured of one or two bubbles, and the suspension was stirred to allow different microstructures to be sampled, but not so vigorous as to introduce air bubbles into the suspension. A discussion of the need for this can be found in Abbott et al.[32] The temperature of the suspension was monitored between trials to limit errors in measurement due to temperature fluctuation.

The path of each bubble meandered, presumably highly influenced by the presence of the suspended particles, as discussed in the context of falling ball rheometry by Abbott et al.[32] Figure 2 shows a reconstructed path from the image processing described in the next subsection. This is a projection into two dimensions of a three-dimensional trajectory because, unfortunately, we could not use multiple X-ray images to reconstruct the full three-dimensional reality. Nevertheless, the shape and size of this projection could be measured, and the deformation of the bubble could be monitored.

Despite the meandering nature of the bubble trajectories, the column was not long enough for a single bubble to sample a statistically significant number of particle spatial arrangements. Thus, a single bubble could not be used to determine an accurate average apparent viscosity of the suspension. Therefore, several tests were performed and combined in a manner similar to that described by Abbott et al.[32] However, the velocities of the bubbles did not appear to vary as much as those of solid balls dropped into similar suspensions. Typically five bubbles were tracked for each suspension along the full length of the test column.

For the suspending liquid and suspensions with concentration $\phi = 0.20$ and 0.30, the shorter length test section column was used for experiments. For these suspensions, the shorter column was of sufficient length for a test bubble to overcome column end effects and reach a steady-state velocity, as will be shown in the next section. The shorter column was found to be of insufficient length for highly concentrated suspensions $\phi = 0.50$, as test bubbles failed to reach a steady terminal velocity within the test section. Test sections of greater length were made to accommodate the larger end effect in the highly concentrated suspensions. The larger test section allowed the bubble to reach a steady terminal velocity as required; however, only part of the test section was visible at one time. Therefore, several bubbles were recorded in one part of the column, the stage moved, and then another set of different bubbles was recorded in the newly visible part of the column. We will discuss the implications of this in a following subsection.

Analysis

Raw bubble data were collected as a series of X-ray images, each time stamped in order to obtain a temporal reference. Temporal resolution for most suspensions was limited to 66 μs, corresponding to a frame rate of 15 fps. System memory limitations required lower frame rates of 7.5 and 5 fps to be used for highly viscous suspensions in order to reduce the amount of raw data. The reduction in temporal resolution was not a serious concern in this case, because the bubbles rose relatively slowly in the highly viscous suspensions.

Spatial calibration was achieved through the use of X-ray images of a perforated steel grid with 0.635-cm diameter holes. The grid was imaged in plane with the center line of the test cylinders. Using the calibration grid, distortion in the X-ray image was found to be less than 2% between any two positions in the image. Spatial resolution was limited by pixel size to 200 μm.

An image sequence of each bubble trial was reconstructed using a commercial image analysis software package, Image-Pro Plus™ (MediaCybernetics). Using automatic tracking features of Image-Pro Plus, the centroid of each bubble was tracked as the bubble traversed the length of the column. The velocity of the bubble was then determined based on the position and time intervals found during the tracking process

at position intervals much larger than the diameter of the suspended spheres.

Bubble size measurements were taken directly from the raw data images. Bubble diameters were determined using the measurement tools of the image analysis software by averaging several measurements of the bubble at a discrete point along the cylinder. This process was repeated as the bubble traversed the cylinder to observe any variation in shape or size due to changes in microstructure or pressure head. For low to moderate suspension concentrations, bubbles were found to be spherical based on the definition that the ratio of major to minor axis must be within 10% of unity.[1] Highly concentrated suspension caused bubbles to be elongated in the direction of gravity as displayed in Figure 3. For purposes of analysis, the bubbles were either approximated as solid spheres (in the case of the low to moderate suspension concentrations) or as prolate spheroids (for highly concentrated suspensions).

Stokes' equation for the velocity of a freefalling solid sphere in the creeping flow regime was used to determine the apparent viscosity of the suspensions based on the velocity of the rising bubble, as if the suspension could be modeled as a hypothetical one-phase Newtonian liquid. Because our experiments use bubbles and not solid test spheres the Stokes' equation was modified based on the Hadamard–Rybczynski solution that assumes a mobile test sphere boundary.[1]

$$\mu = \frac{1}{12}\frac{d_f^2 g(\rho_s - \rho_a)}{vK_{wall}},$$

where d_f is the bubble diameter, ρ_s is the density of the suspension, ρ_a is the density of the test bubble, v is the bubble rise velocity, and K_{wall} is the correction factor for containing cylinder wall effects. This equation is valid for Reynolds number <1.[1] For our experiments, the average Reynolds number (based on the bubble diameter) was $Re = 0.035$ with a maximum of $Re = 0.097$. Known values of density and gravitational acceleration g were used along with the measured bubble diameter and velocity to find the apparent viscosity at each location along the axis of the containing cylinder. This allowed comparison among data taken with slightly different bubble sizes. The wall correction factor used to modify Stokes' equation is given by Haberman and Sayre for a circulating sphere traversing the length of a cylinder along the axis of the cylinder[1]:

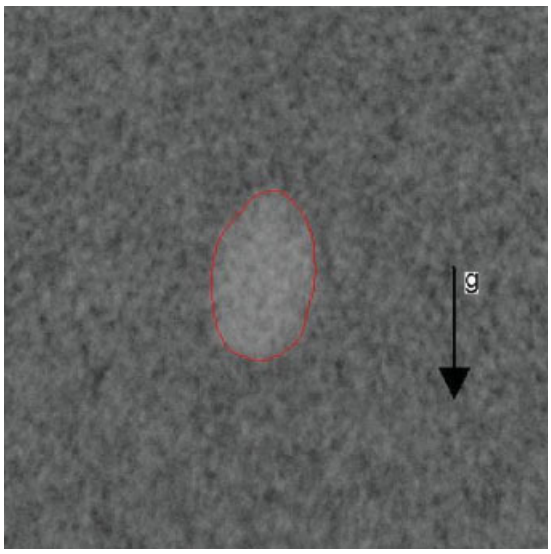

Figure 3. X-ray image of a bubble rising in a suspension with 50% of solid spheres by volume.

[Color figure can be viewed in the online issue, which is available at www.interscience.wiley.com.]

$$K_{wall} = \frac{1 + 2.2757\left(\frac{1-\kappa}{2+3\kappa}\right)\lambda^5}{1 - 0.7017\left(\frac{2+3\kappa}{1+\kappa}\right)\lambda + 2.0865\left(\frac{\kappa}{1+\kappa}\right)\lambda^3 + 0.5689\left(\frac{2-3\kappa}{1+\kappa}\right)\lambda^5 - 0.72603\left(\frac{1-\kappa}{1+\kappa}\right)\lambda^6},$$

where $\lambda = d_f/D$ and D is the cylinder diameter. For a gas bubble in a viscous liquid, $\kappa = 0$. This equation was found to be valid for low Reynolds number flows up to $\lambda = 0.6$. For our experiments, λ was limited to 0.41.

As mentioned above, for highly concentrated suspensions of $\phi = 0.50$, the test bubbles assumed a prolate spheroid shape, as displayed in the X-ray image Figure 3. To correct for this deviation in spherocity Stokes' equation was further modified.

$$\mu = \frac{1}{3}\frac{abg(\rho_s - \rho_a)}{vK_{wall}K_{shape}},$$

where a is the polar bubble radius, b is the equatorial bubble radius, and K_{shape} is the correction to Stokes' equation for a spheroidal shaped falling body. In addition to the wall correction factor given by Haberman and Sayre, this second correction factor was used to correct for the change in shape of the test bubble.[33]

$$K_{shape} = \left[\frac{3}{4}\sqrt{\tau_0^2 - 1}\left[\left(\tau_0^2 + 1\right)\coth^{-1}\tau_0 - \tau_0\right]\right]^{-1}$$

$$\text{where} \quad \tau_0 = \left[1 - \left(\frac{b}{a}\right)^2\right]^{-1/2}.$$

This correction factor accounts for the increased drag felt by a prolate spheroid moving parallel to its major axis relative to the drag felt by a sphere of equal equatorial radius.

For purposes of comparison, the apparent viscosities of each suspension had to be normalized to remove viscosity variances due to suspending fluid type and temperature. To

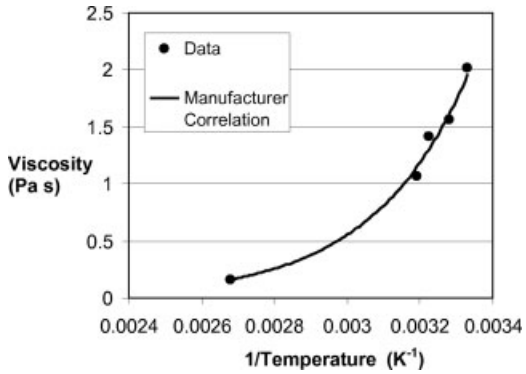

Figure 4. Ucon 50-HB-5100 bubble-measured viscosity compared with manufacture's published viscosity.

do this, first we obtained the pure fluid ($\phi = 0$) viscosity using the same rising bubble technique at various temperatures covering the full range of temperatures experienced by the suspensions in our experiments. The subsequently measured suspension viscosities were then normalized based on the pure suspending fluid viscosity at the corresponding temperature, as

$$\mu_r = \frac{\mu_s}{\mu_o},$$

where μ_r is the relative viscosity, μ_s is the apparent suspension viscosity, and μ_o is the viscosity of the suspending fluid at the conditions of the experiment.

The results from individual bubbles in the same suspension were combined and averaged to find a mean "instantaneous" apparent viscosity as a function of the position in the cylinder. In each trial, the region in the cylinder characterized by essentially no change in the mean apparent viscosity (and hence, free from end effects) was identified. In this region, the "instantaneous" viscosities were averaged to obtain a single mean steady-state apparent viscosity for a particular suspension.

Validation of experimental method

The viscosity of each pure suspending fluid was determined through multiple bubble test trials. The viscosity was calculated using the terminal velocity of the bubbles based on the Hadamard–Rybczynski solution for a spherical fluid particle in creeping flow as described in the previous subsection. Viscosities were found for Ucon 50-HB-5100 at multiple temperatures based on this method. Figure 4 shows that the results are in good agreement with the manufacture's published data. Thus the equation for mobile surfaces was found to be consistent with the data unlike that for a fixed boundary, giving more evidence that surface-active agents that could reduce mobility were not present.

To ensure that bubbles injected into the suspensions were not altering the microstructure in such a way that would cause a change in the velocity profiles of subsequent bubbles, the velocities of multiple bubbles were found without stirring the suspensions. After an initial stirring of the test suspension, a bubble would be injected and its velocity tracked. Then, after many other bubbles had been injected at the regular interval chosen for the bubble generator, another bubble would be tracked to see if the continuous stream of bubbles significantly altered the velocity of the final bubble from that of the first. Figure 5 shows typical examples of the comparison of velocities of an initial and a subsequent bubble in the first imaging section (closest to the bottom), subject to the conditions above in both the suspending fluid and suspensions. Qualitative examination of the results shown in Figure 5a leads one to conclude that the two bubbles essentially experienced the same initial acceleration and had similar velocity profiles.

We expected that the bubble passage could possibly rearrange small particles more easily than larger ones, affecting the apparent viscosity felt by subsequent bubbles. However, Figure 5b shows that variations in the suspensions of the largest particles are more pronounced. This perhaps should not be surprising considering the natural variations expected in such complex systems, where slight differences in initial conditions can eventually lead to large differences in the

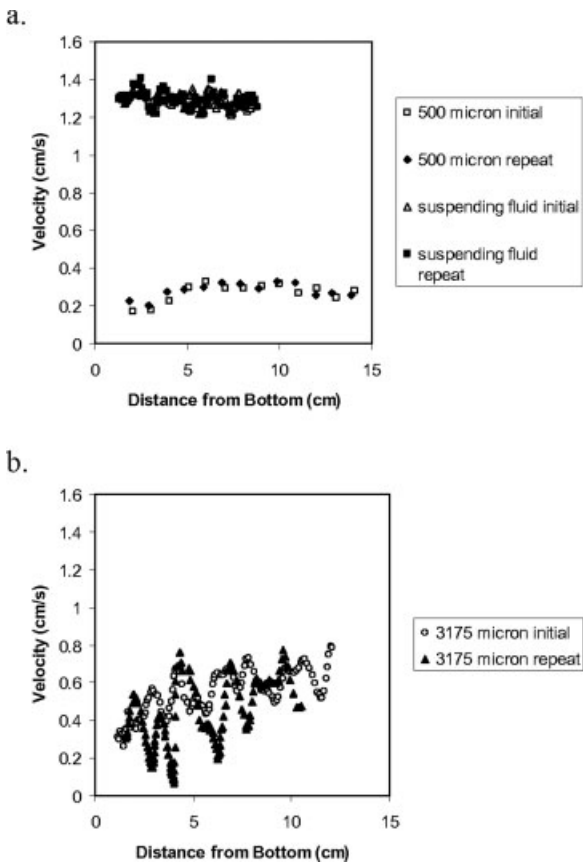

Figure 5. a) Bubble velocity repeatability during continuous stream of bubbles through the single-phase suspending liquid and a suspension of 50% of 500 μm diameter particles. b) Bubble velocity repeatability during continuous stream of bubbles through a suspension of 50% of 3175 μm diameter particles.

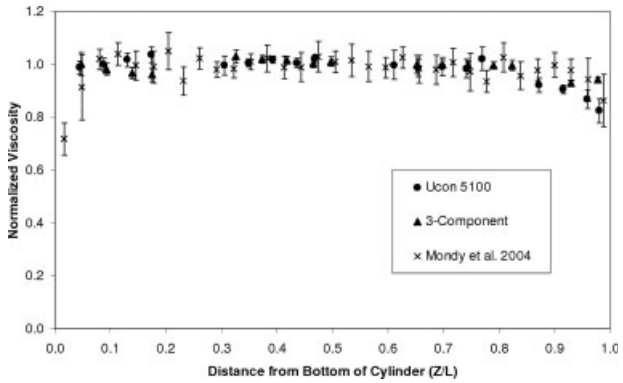

Figure 6. Bubble behavior in Newtonian liquids.

trajectories. Because we could not eliminate the possible effects of velocity changing with time, and because we were interested in the average end effects, we alternated taking measurements first at the bottom of the cylinder and traversing the measurement zone upward and starting at the top section and traversing the zone downward.

Results

Effect of height of contained suspension

Figure 6 shows the results for bubbles rising in two Newtonian suspending liquids, either Ucon 50-HB-5100 or the three-component system, with no suspended particles present. The liquids are held in a cylinder with diameter $D = 4.4$ cm and height $L = 52$ cm. These measured viscosities as a function of the distance Z from the bottom of the cylinder are derived from the average of five bubbles and are compared to the measurements taken by Mondy et al. of a similar three component fluid held in a cylinder with $D = 3.7$ cm and $L = 83.6$ cm.[28] To compare the viscosities found in these experiments, each viscosity measurement is normalized by the mean viscosity of that fluid obtained by averaging the values obtained with $0.2 < Z/L < 0.7$. The error bars shown on the figure are the 95% confidence limits based on Student's t-distribution and reflect the random experimental error in bubble generation and measurements. The bubbles achieve a steady-state velocity within a little over one cylinder diameter D in the earlier data and within the first measurement zone of height $0.5D$ using the X-ray system. As they come within about $2D$ of the top ($4D$ for the earlier data), they accelerate by about 10–20%. We do not expect the end effects to be identical between the earlier data and the present data, because the earlier data were taken at conditions with a combination of Reynolds and Bond numbers that puts them on the border of the ellipsoidal/spherical cap regime.[1] High-speed video of the earlier experiments are not available, so the shape could not be confirmed. The bubbles in the current experiments are spherical.

In concentrated suspensions, the bubbles experienced added resistance attributed to the presence of the cylinder bottom, as has been seen in earlier falling ball experiments and the earlier bubble rise experiments.[26,28] Figure 7 shows that in the suspension with a volume fraction of particles of 0.50, a bubble does not reach a steady velocity until about $14D$. As the volume fraction of solid particles decreases, the end effects become less dramatic, and bubbles achieved steady state within $4D$ when $\phi = 0.30$. Here, each set of experiments tested 500 μm suspensions in 4.4-cm diameter cylinders. Again the points indicate averages over measurements for five bubbles. The measured viscosity has been normalized by the steady-state viscosity for each suspension to emphasize the end effects. The actual measured viscosity varies dramatically with ϕ, as will be discussed in a following subsection. Notice also that the distribution of velocities as reflected in the 95% confidence limits is smaller in the less concentrated suspensions. This has also been observed with falling balls.[32]

Because of the enhanced effect of the bottom observed in these suspensions, any measurements designed to determine the viscosity of a suspension as an effective Newtonian media must be taken in sufficiently long cylinders. In the following studies, the most concentrated suspensions were always held in a cylinder with an L/D of at least 20.

Effect of the size of the suspended spheres on the end effects

Figure 8 shows the measured viscosities averaged over five bubble trajectories along the axis of the containing cylinders ($D = 4.4$ cm) for two suspensions with $\phi = 0.50$, either made up of 500- or 3175-μm diameter spheres. Within the confidence limits of the data, the end effects are not significantly affected by the relative size of the suspended spheres to the bubble. However, the measured viscosity of the suspension of large particles is lower than that measured in the suspension of small particles. Therefore, the viscosities are plotted normalized by the steady-state viscosity (the average of the measurements at $Z/D > 15$). We will discuss how the absolute viscosity varies in the next subsection. Two moderately concentrated suspensions of $\phi = 0.30$, varying only by the size of the suspended particles, also exhibited end effects similar to within the limits of uncertainty.

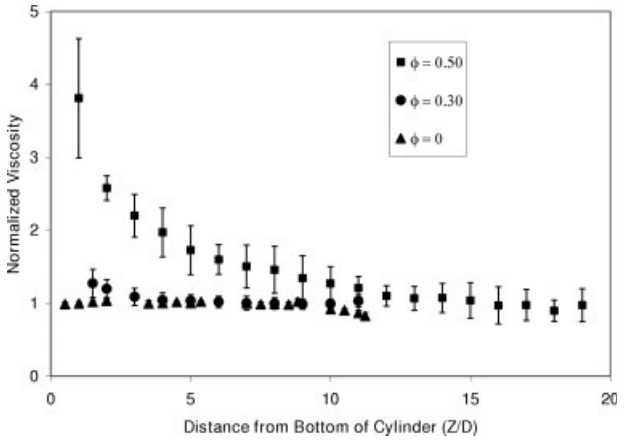

Figure 7. Viscosity profiles normalized by the steady-state viscosity for each suspension.

Suspensions contain 500 μm polystyrene at various particle concentrations and are tested in 4.4 cm-diameter cylinders.

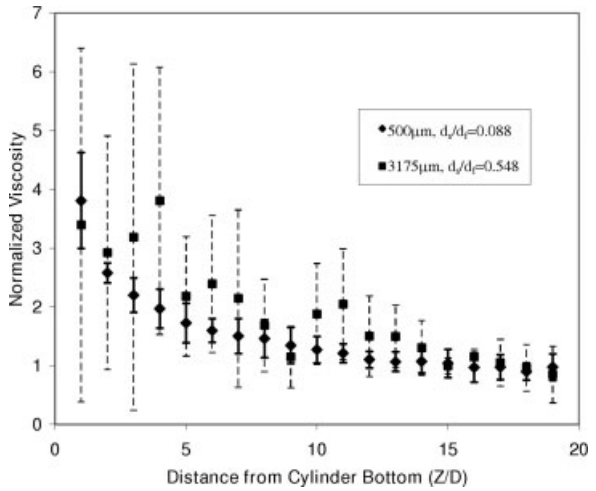

Figure 8. End effects in two suspensions with $\phi = 0.50$ but with different sized particles.

The confidence limits for the larger particle size (dashed bars) are much longer than for the smaller particle size and reflect the greater variation in velocities seen when the suspended particles are comparable in size to the rising bubble.

Effect of the size of the suspended spheres on the bubble rise velocity

Figure 9 shows the measured viscosities along the axis of the containing cylinders for four suspensions with $\phi = 0.50$ of various sizes of suspended spheres, identified by the ratio of suspended sphere diameter d_s to the diameter of the rising bubble d_f. Here, the measured velocities are normalized by the suspending fluid viscosity to obtain relative viscosities, not by the respective steady-state viscosities as in Figure 8. In general, as the particle size goes up relative to the bubble size, the steady-state viscosity goes down. This is consistent with previously reported data using falling balls[16] and rising bubbles in fluidized beds.[11] Although the viscosity profiles are similar in shape for each suspension, it is not immediately apparent that a trend exists describing the variations in the profiles.

It has been shown in falling ball experiments in highly concentrated suspensions that the apparent relative viscosity of a suspension is insensitive to changes in the diameter of the falling ball when the ratio of sizes of the suspended spheres and the falling ball (d_s/d_f) are in the range between 0.166 and 0.5.[16,34–36] Here, the relative viscosity is also insensitive to changes in cylinder diameter as long as the cylinder diameter is at least 46 times larger than the diameter of the suspended spheres. We will call this region where the viscosity is insensitive to test sphere size the "Newtonian plateau." A decrease in relative viscosity has been observed as the falling ball becomes small compared to the suspended spheres; however, this particular region is outside of the parameters of the current study. However, falling ball experiments in the region below the d_s/d_f limits above have been found to result in an increase in the measured relative viscosity over that of the Newtonian plateau value. This appears to be an effect of the confining cylinder diameter.

To try to understand the effects that are important in Figure 9, we performed tests in additional cylinders of various diameters. Figure 10 is a plot of the relative viscosity of three separate concentrations of suspended particles both within and below the limits of the Newtonian plateau found in falling ball experiments. We have also included points from the earlier data,[28] where we estimate from the size and speed that the bubble was spherical or prolate, with a mobile surface, and we reanalyze these data as in our current study.

As seen in Figure 10, the relative viscosity of both the $\phi = 0.20$ and $\phi = 0.30$ suspensions is not affected significantly by the variation in particle to rising bubble size ratio. Conversely, the highly concentrated suspension $\phi = 0.50$ exhibits a marked increase over the Newtonian relative viscosity as the particles become small compared to the rising bubble, as indicated by the lines drawn through the data in Figure 10. These lines slope upward as the ratio d_s/d_f

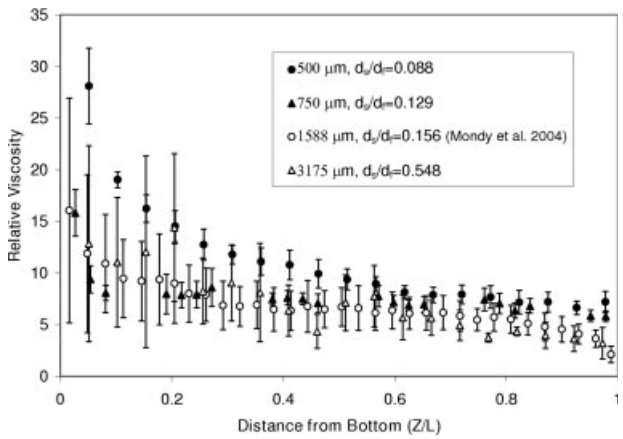

Figure 9. Apparent viscosity measured at different heights in various cylinders containing suspensions of solid volume fraction 0.50 of spheres with various radii.

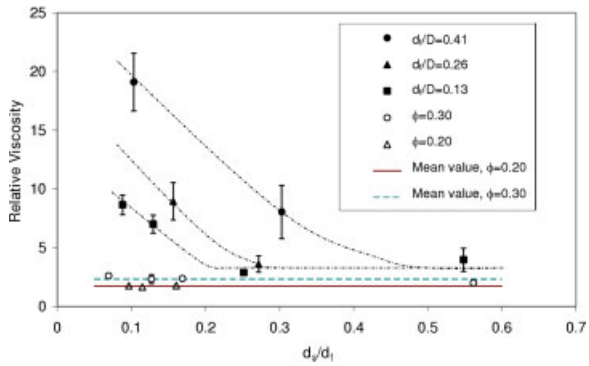

Figure 10. Effect of relative bubble size on relative viscosity for various suspended particle concentrations.

Solid points represent $\phi = 0.50$. Data for $\phi = 0.20$ are from Mondy et al. (2004) reanalyzed for bubbles with mobile surfaces. Also from Mondy et al. (2004) (reanalyzed) are points at $d_s/d_f = 0.10$ and $d_s/d_f = 0.156$ with $\phi = 0.50$. Dotted lines through the $\phi = 0.50$ data are to guide the eye. [Color figure can be viewed in the online issue, which is available at www.interscience.wiley.com.]

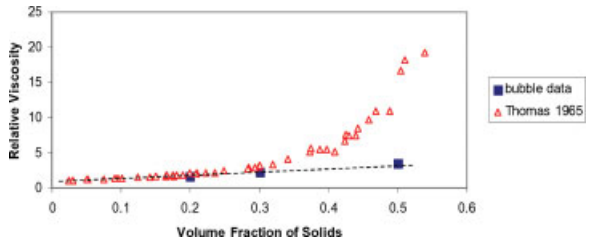

Figure 11. Apparent viscosity felt by a bubble compared to literature values.

[Color figure can be viewed in the online issue, which is available at www.interscience.wiley.com.].

decreases from the Newtonian region. Although there is insufficient data to make a quantitative assessment, the lower limit of the Newtonian region is dependant on the rising bubble to cylinder diameter ratio d_f/D. For $d_f/D = 0.13$ the lower limit of the Newtonian plateau is below $d_s/d_f = 0.25$. This lower limit increases to $d_s/d_f \approx 0.5$ or 0.6 as d_f/D increases 0.41. Sensitivity of the relative viscosity to d_f/D has also been observed for falling ball experiments.[34–36]

From Figure 10, we can determine the relative viscosity that would be felt by a bubble (with the size within our range), without the effects of the confining cylinder, as a function of the suspended particle concentration. We average the results for $\phi = 0.20$ and for $\phi = 0.30$, and for the points within the Newtonian plateau for $\phi = 0.50$. Figure 11 compares these points to a fit of suspension viscosity measured with conventional torsional rheometers.[37] One can see that the apparent viscosity felt by the bubbles is approximately linear with ϕ, increasing far less than the rheometer data.

Discussion

Far from the cylinder ends, the apparent viscosity of a moderately concentrated suspension ($\phi = 0.30$) as felt by a rising bubble is insensitive to the relative sizes of the bubble and the suspended particles. Also, wall effects developed for spherical bubbles moving through single-phase Newtonian fluids approximate well the wall effects in moderately concentrated suspensions over a range of particle and bubble sizes, as shown by the ability of the rising bubble's velocity to predict the suspension viscosity measured with other rheometer types (Figure 11). However, in these suspensions Newtonian end effects are not valid. The bubbles are influenced by the bottom over a much greater distance than in the suspending fluid alone, and this enhancement of the end effects increases as the concentration of particles increases.

This increase in end effects is consistent with falling ball studies reported recently, in which it was argued that the enhanced end effects seen with solid falling balls could be attributed to either (1) an effective hydrodynamic percolation limit existing between the ball and the containing walls of the cylinder and/or (2) small inertial effects leading to restrictions in the recirculation of the suspension off the bottom.[26] In the former case, the suspended particles may form effective chains connecting the nearest neighbors of the bubble to the containing walls, including the bottom, and adding resistance to the motion of the bubble. In the latter, it was argued that recirculation of the suspension near the bottom of the cylinder was restricted by small, but finite, inertial forces, and that larger balls could more easily push aside the suspended spheres in their path leading to a smaller enhancement of end effects than that experienced by the smaller balls. In both arguments, bubbles would seem less likely than solid falling balls to break the chains or push aside suspended particles. However, the enhanced end effects remain approximately the same as those measured with comparably sized solid spheres. If the dominant effect is described by the latter argument, it is possible that the small solid spheres used by Reardon and coworkers were already below a critical Stokes number to give a maximum in the end effects. However, the fact that the suspension imparted a similar effect on the bubbles leads us to believe that the enhanced end effects are more likely to be caused by a percolation limit that only depends on the sizes of the suspended particles, containing cylinder, and tracer particle (in this case a bubble). As stated previously by Reardon and coworkers, these studies should encourage the detailed examination of suspension microstructure, either numerically or experimentally, to determine the true nature of the observed enhancement of end effects.

At higher concentrations of suspended particles ($\phi = 0.50$), other effects are present, also. First, the bubbles elongate, which we believe to be due either to the non-Newtonian nature of the suspension or to a percolation effect that essentially creates confining "walls" closer to the bubble than are the actual cylinder walls. Elongation of bubbles confined to narrow cylinders have been observed in both Newtonian and non-Newtonian fluids.[29] Teardrop shaped bubbles have been observed in viscoelastic fluids.[30,38] Although the suspensions here are created with Newtonian suspending liquids, we expect them to exhibit normal forces at the highest concentrations.[39] Although the bubbles here do not appear to be teardrop shaped, the resolution of the X-ray images are not good enough say for certain that there are no tails.

Newtonian cylinder wall effects are valid as long as $d_s/d_f > 0.4$ and $d_f/D > 0.13$. Below these limits enhanced wall effects may occur, resulting in higher apparent suspension viscosities. Previous studies of solid balls falling through suspensions have observed similar phenomena.[16,26] However, here the falling balls tend to push the suspended particles out of the way. The "large ball effect," where enhanced wall effects occur, was thought to occur in situations where the ball could no longer freely move the highly confined suspended particles. This is consistent with the observation of bubble deformation.

Finally, bubbles travel faster than would be predicted in concentrated suspensions based on the expected suspension apparent viscosity as reported in the literature.[37] Observations possible with the radiography showed us that, especially in the highly concentrated suspensions of the largest particles, the passage of bubbles moved the suspended particles less than a similarly sized solid ball falling through the suspension did. The bubbles deformed (occasionally grossly) and could be seen to weave around the largest suspended particles. This is consistent with the observation that the passage of many bubbles did not unduly increase the velocity of the latter ones. Although the qualitative agreement with wall effects is seen in falling ball rheometry, the resulting apparent viscosity of the highly concentrated suspensions seen with the bubbles is far less. This could be because the

bubbles deform the suspension microstructure less than would a solid ball. However, the bubbles in the moderately concentrated suspensions do remain spherical and, because the particle spacing even at these lower concentrations is smaller than the bubble size, the bubbles must deform the suspension microstructure. Here, the apparent viscosities calculated from the bubble velocities and those calculated from the solid ball velocities are closer in value.

Acknowledgments

Sandia is a multiprogram laboratory operated by Sandia Corporation, a Lockheed Martin Company for the United States Department of Energy's National Nuclear Security Administration under contract DE-AC04-94AL85000. Work performed at Los Alamos National Laboratory was sponsored by the U.S. Department of Energy under contract W-7405-ENG-36 with the University of California. Partial support for this work was provided by the D.O. E. Office of Science, Advanced Computing Research (ASCR) program in Applied Mathematical Sciences.

Literature Cited

1. Clift R, Grace JR, Weber ME. *Bubbles, Drops, and Particles*. New York: Academic, 1978.
2. Fan L-S, Tsuchiya K. *Bubble Wake Dynamics in Liquids and Liquid-Solid Suspensions*. Boston: Butterworth-Heinemann, 1990.
3. Chhabra RP. *Bubbles, Drops and Particles in Non-Newtonian Fluids*, 2nd ed. Ann Arbor: CRC Press, 2006.
4. Sokolichin A, Eigenberger G, Lapin A. Simulation of buoyancy driven bubbly flow: established simplifications and open questions. *AIChE J*. 2004;50:24–45.
5. Jameson GJ, Nam S, Young MM. Physical factors affecting recovery rates in flotation. *Miner Sci Eng*. 1977;9:103–118.
6. Yoon R-H. The role of hydrodynamic and surface forces in bubble-particle interaction. *Int J Miner Proc*. 2000;58:129–143.
7. Phan CM, Nguyen AV, Miller JD, Evans GM, Jameson GJ. Investigations of bubble-particle interactions. *Int J Miner Proc*. 2003;72: 239–254.
8. Fan L-S. *Gas-Liquid-Solid Fluidization Engineering*. Boston: Butterworths, 1989.
9. Darton RC, Harrison D. The rise of single gas bubbles in liquid fluidized beds. *Trans Inst Chem Eng*. 1974;52:301–306.
10. Tsuchiya K, Furumoto A. Tortuosity of bubble rise path in a liquid-solid fluidized bed: effect of particle shape, *AIChE J*. 1995;41:1368–1374.
11. Tsuchiya K, Furumoto A. Fan L-S, Zhang J. Suspension viscosity and bubble rise velocity in liquid-solid fluidized beds. *Chem Eng Sci*. 1997;52:3053–3066.
12. Li H, Prakash A. Influence of slurry concentrations on bubble population and their rise velocities in a three-phase slurry bubble column. *Powder Technol*. 2000;113:158–167.
13. Zhang J, Li Y, Fan, L-S. Discrete phase simulation of gas-liquid-solid fluidization systems: single bubble rising behavior. *Powder Technol*. 2000;113:310–326.
14. Buwa VV, Ranade VV. Dynamics of gas-liquid flow in a rectangular bubble column: experiments and single/multi-group CFD simulations. *Chem Eng Sci*. 2002;57:4715–4736.
15. Kenny TA, McLaughlin JB. Bubble motion in three-phase liquid fluidized bed. *Chem Eng Commun*. 1999;172:171–188.
16. Mondy LA, Graham AL, Jensen JL. Continuum approximations and particle interactions in concentrated suspensions. *J Rheol*. 1986;30: 1031–1051.
17. Poletto M, Joseph DD. Effective density and viscosity of a suspension. *J Rheol*. 1995;39:323–343.
18. Bohlin T. The drag on a rigid sphere moving in a viscous liquid inside a cylindrical tube. *Trans R Inst Tech*. 1960;155:1–63.
19. Haberman WL, Sayre RM. David Taylor Model Basin Report No. 1143, U.S. Navy, Washington, DC, 1958.
20. Tanner RI. End effects in falling-ball viscometry. *J Fluid Mech*. 1963;17:161–170.
21. Chhabra P, Uhlherr PHT. The influence of fluid elasticity on wall effects for creeping sphere motion in cylindrical tubes *Can J Chem Eng*. 1988;66:154–157.
22. Graham AL, Mondy LA, Miller JD, Wagner NJ, Cook WA. Numerical simulations of eccentricity and end effects in falling ball rheometry. *J Rheol*. 1989;33:1107–1128.
23. Wham RM, Basaran OA, Byers CH. Wall effects on flow past fluid spheres at finite Reynolds number: wake structure and drag correlations. *Chem Eng Sci*. 1997;52:3345–3367.
24. Higdon JJL, Muldowney GP. Resistance functions for spherical particles, droplets and bubbles in cylindrical tubes. *J Fluid Mech*. 1995; 298:193–210.
25. Kaiser AE, Graham AL, Mondy LA. Non-Newtonian wall effect in concentrated suspensions. *J Non-Newtonian Fluid Mech*. 2004; 116:479–488.
26. Reardon P. Constant force and constant velocity experiments in concentrated suspensions. PhD Dissertation, Texas Tech University, Lubbock, Texas, 2003.
27. Reardon PT, Chawla V, Admuthe RS, Feng S, Graham AL, Mondy LA. Non-Newtonian end effects in falling ball viscometry of concentrated suspensions. *Rheol Acta*. 2007;46:413–424.
28. Mondy LA, Grillet AM, Chawla V, Graham AL. Dynamics of a bubble rising through a suspension of solid particles. In: *Proceedings of the XIVth International Congress on Rheology*, August 22–27, Seoul, Korea, 2004.
29. Coutanceau M, Hajjam M. Viscoelastic effect on the behaviour of an air bubble rising axially in a tube. *Appl Sci Res*. 1982;38:199–207.
30. Acharya A, Mashelkar RA, Ulbrecht J. Mechanics of bubble motion and deformation in non-Newtonian media. *Chem Eng Sci*. 1977;32:863–872.
31. Abbott JR, Tetlow N, Graham AL, Altobelli SA, Fukushima E, Mondy LA. Stephens TS. Experimental observations of particle migration in concentrated suspensions: Couette flow. *J Rheol*. 1991; 35:773–794.
32. Abbott JR, Graham AL, Mondy LA, Brenner H. Dispersion of a ball settling through a quiescent neutrally buoyant suspension. *J Fluid Mech*. 1998;361:309–331.
33. Happel J, Brenner H. *Low Reynolds Number Hydrodynamics*. Boston: Martinus Nijhoff Publishers, 1983.
34. Milliken WJ, Mondy LA, Gottlieb M, Graham AL, Powell RL. The effect of the diameter of falling balls on the apparent viscosity of suspensions of spheres and rods. *PhysicoChem Hydrodyn*. 1989; 11:341–355.
35. Mor R, Gottlieb M, Graham AL, Mondy LA. Viscosity of concentrated suspensions of sphere/rod mixtures. *Chem Eng Commun*. 1996;150:421–430.
36. Mondy LA., Graham AL, Gottlieb M. Microrheological observations on the onset of non-newtonian behavior in suspensions. In: *Proceedings of the Xth International Congress on Rheology*, August 14–19, Sydney, Australia, 1988.
37. Thomas DG. Transport characteristics of suspensions. VIII. A note on the viscosity of Newtonian suspensions of uniform spherical particles. *J Colloid Sci*. 1965;20:267–277.
38. Astarita G, Apuzzo G. Motion of gas bubbles in non-Newtonian liquids. *AIChE J*. 1965;11:815–820.
39. Zarraga IE, Hill DA, Leighton DT. The characterization of the total stress of concentrated suspensions of noncolloidal spheres in Newtonian fluids. *J Rheol*. 2000;44:185–220.

Manuscript received May 21, 2007, revision received Oct. 28, 2007, and final revision received Dec. 29, 2007.